МЕХАНИКА
MECHANICS

UDC 622.692.4
https://doi.org/10.23947/2687-1653-2024-24-2-135-147

Original Theoretical Research

Analysis of the Drag-Reduction Ability of the Layout and Cross-Sectional Shapes of Subsea Structures in the Critical Flow Mode

Henry F. Annapeh, **Victoria A. Kurushina** ✉
Industrial University of Tyumen, Tyumen, Russian Federation
✉ v.kurushina@outlook.com

EDN: TDJYXD

Abstract

Introduction. Slender structures of subsea energy production systems are under constant influence of currents and waves. Hydrodynamic loads result from the interaction of subsea pipelines, umbilicals, equipment supports with fluid flows, and lead to the vortex formation in the area behind the structures. Vortex-induced forces are the sources of the cyclic loading. They accelerate gradually the fatigue damage, which may result in a failure. One of the ways to reduce the loads on subsea structures is to alter the shape of a cross-section, taking into account the flow regime. Dependence of the resulting hydrodynamic loads on the cross-sectional shape and relative position of structures has not been studied in details for the uniform flow in the critical mode. The current work is aimed at filling this gap. The research objective is to consider the impact of the distance between the structures, and also, the presence of a D-shaped structure, placed upstream relative to the group of three cylinders of different cross-sectional shapes.

Materials and Methods. The computational fluid dynamics approach was used in this work for numerical simulations of vortex-induced forces in the ANSYS Fluent software for cylinder with D = 0.3 m. Modelling was conducted with the Detached Eddy Simulation (DES) method, which combined advantages of the Reynolds-averaged Navier-Stokes equation (RANS) method and the Large Eddy Simulation (LES) method. The object of the research was the system of four structures in the 2D computational domain, which included the upstream D-shaped cylinder and the main group of three cylinders with the circular, squared and diamond shapes of the cross-section. The transient process was considered, where structures were under the influence of the uniform flow in the critical regime at $Re = 2.5\times10^5$.

Results. Five sets of data were obtained in simulations for the time-dependent coefficients of the lift and drag forces: for the main system — of the D-shaped, circular, square and diamond structures, and also for the four systems — of only D-shaped, only circular, only square and only diamond shaped structures. Additional analysis was conducted for the effect of the distance between the structures on the amplitude of fluctuating hydrodynamic force coefficients. The obtained results are presented as time histories of coefficients of the lift and drag forces, frequency analysis and contours of velocity, pressure and vorticity fields. The results indicate a positive effect of the upstream D-shaped structure on reducing the drag force, acting on the central structure in the group of three cylinders located downstream.

Discussion and Conclusion. The results of the performed studies facilitate the informed decisions regarding the arrangement of subsea structures in a group of four objects, depending on the cross-sectional shape and the distance between the structures. The upstream D-shaped structure provides reducing the hydrodynamic drag force acting on the central structure in the downstream group of three structures, thereby slowing the fatigue accumulation and increasing the time of safe operation.

Keywords: vortex-induced forces, drag coefficient, lift coefficient, uniform flow

Acknowledgements. The authors would like to thank Dr. A. Postnikov for the discussion on simulation of the flow over cylinder. The authors also thank the Editorial Board of the Journal and the anonymous reviewers for the constructive comments, which helped improving the paper.

Funding Information. The research is done with the financial support of the National Project “Science and Universities” from the Ministry of Science and Higher Education of the Russian Federation (grant no. FEWN–2021–0012).

For Citation. Annapeh HF, Kurushina VA. Analysis of the Drag-Reduction Ability of the Layout and Cross-Sectional Shapes of Subsea Structures in the Critical Flow Mode. *Advanced Engineering Research (Rostov-on-Don).* 2024;24(2):135–147. https://doi.org/10.23947/2687-1653-2024-24-2-135-147

Оригинальное теоретическое исследование

Анализ возможности снижения лобового сопротивления за счёт расположения и поперечных сечений подводных конструкций в потоке критического режима

Г.Ф. Аннапе, **В.А. Курушина** ✉
✉ v.kurushina@outlook.com

Аннотация

Введение. Длинные и узкие в поперечнике конструкции морских энергодобывающих систем находятся под постоянным воздействием течений и волн. Гидродинамические нагрузки являются результатом взаимодействия подводных трубопроводов, шлангокабелей, опор оборудования с потоком жидкости и приводят к образованию вихрей в зоне за конструкциями. Вихреобразовательные силы служат источником циклического нагружения и постепенно ускоряют усталостное разрушение, что может привести к авариям. Одним из способов снижения нагрузок на подводные конструкции является изменение формы их поперечного сечения с учетом режима потока. Недостаточно изучено, каким образом итоговые гидродинамические нагрузки зависят от формы поперечного сечения и взаимного расположения названных выше элементов систем, находящихся в равномерном критическом потоке. Представленная научная работа призвана восполнить этот пробел. Цель исследования — рассмотреть в данном контексте значение расстояния между конструкциями, а также наличие полукруглой D-образной конструкции, размещённой перед группой из трёх цилиндров с разными поперечными сечениями.

Материалы и методы. Для численного моделирования вихреобразовательных сил использовался метод вычислительной динамики флюидов в программе ANSYS Fluent для цилиндров диаметром D = 0,3 м. Моделирование выполнено методом неприсоединённых вихрей DES, который сочетает в себе преимущества метода усреднённого по Рейнольдсу уравнения Навье-Стокса RANS и метода крупных вихрей LES. В качестве объекта исследования рассматривалась система, состоящая из четырёх конструкций в вычислительном домене в 2D, включая стоящий выше по течению полукруглый цилиндр и основную группу из трёх цилиндров круглой, квадратной и ромбовидной формы поперечного сечения. Эти конструкции в условиях неустановившегося процесса находятся под действием равномерного потока критического режима при $Re = 2{,}5 \times 10^5$.

Результаты исследования. В результате моделирования получены пять наборов данных для изменяющихся во времени коэффициентов вихреобразовательных подъёмной силы и силы сопротивления: для основной системы из полукруглой, круглой, квадратной и ромбовидной конструкции, а также для четырёх систем из только полукруглых, только круглых, только квадратных и только ромбовидных конструкций. Дополнительно проведён анализ влияния расстояния между конструкциями на амплитуду колебаний коэффициентов гидродинамических сил. Полученные результаты представлены в виде коэффициентов подъёмной силы и силы сопротивления в динамике, анализа частот и контуров полей скорости, давления, завихрённости. Результаты позволяют установить положительное влияние стоящей выше по течению полукруглой конструкции на снижение силы сопротивления на центральную конструкцию в группе из трёх цилиндров ниже по течению.

Обсуждение и заключение. Результаты проведённых исследований позволяют принимать обоснованные решения для расстановки морских конструкций в группе из четырёх объектов в зависимости от формы поперечного сечения и расстояния между ними. Установка полукруглой конструкции выше по течению позволяет снизить гидродинамическую силу сопротивления на центральную конструкцию в группе из трёх конструкций ниже по течению, что замедляет её усталостное разрушение и увеличивает срок эксплуатации.

Ключевые слова: вихреобразовательные силы, коэффициент лобового сопротивления, коэффициент подъемной силы, равномерный поток

Благодарности. Авторы выражают признательность доктору А. Постникову за обсуждение по моделированию потока вокруг цилиндра. Авторы также благодарят редакционную коллегию журнала и анонимных рецензентов за конструктивные замечания, позволившие улучшить статью.

Финансирование. Исследование выполнено при финансовой поддержке Национального проекта «Наука и университеты» Министерства науки и высшего образования Российской Федерации (грант номер FEWN–2021–0012).

Для цитирования. Аннапе Г.Ф., Курушина В.А. Анализ влияния расположения конструкций и поперечных сечений на снижение лобового сопротивления в условиях критического потока. *Advanced Engineering Research (Rostov-on-Don).* 2024;24(2):135–147. https://doi.org/10.23947/2687-1653-2024-24-2-135-147

Introduction. Operation and construction of modern offshore systems, specializing on the energy production, extraction of resources or carbon capture and storage, require evaluation of the impact of environmental flows on equipment and structures. An increased fatigue failure in subsea structures, such as pipelines, risers, cables, piles, equipment supports, may come from the vortex shedding phenomenon. The problem is particularly important when slender structures are designed to reach deep waters to connect subsystems together. The layout of subsea systems comes with the arrangement of structures with different geometry, hydrodynamic properties, and their position in proximity to each other. The interference of wakes from these structures and vortex formation patterns is sometimes challenging to predict at very high Reynolds numbers due to the turbulent nature of the flow.

Differences in the flow over a standalone cylinder and two cylinders in tandem are discussed in [1], and three vortex shedding regimes are identified for tandem structures. These vortex formation modes include the extended-body regime at $1.0 < L/D < 1.8$, where L/D is spacing ratio, commonly used to quantify the distance between centres of neighbour structures. So that, L corresponds to the distance, and D is the diameter of the structure. In [1], increase of the spacing ratio to $1.8 < L/D < 3.8$ leads to the reattachment regime, where shear layers detach from the upstream structure and reattach to the front side of the downstream structure, so that vortices are formed behind this downstream object. Further growth of the spacing ratio, above $L/D > 3.8$, introduces the co-shedding regime, where a separate vortex is formed from the upstream structure and from the downstream structure. Another fundamental research investigated vortex dynamics in details through experimental research [2]. One of the following fundamental studies [3] experimentally investigated the vortex shedding frequencies of two staggered identical circular cylinders with the Reynolds number Re varying from 3.2×10^4 to 7.4×10^4, and two fixed side-by-side cylinders at the Reynolds number of 2.5×10^4 were earlier considered in [4]. These investigations provide an important foundation for modern studies in terms of the known effects in fluid forcing and vortex shedding patterns.

Significantly more recent investigations are performed numerically [5] to study the effect of spacing on loads and vibrations for two tandem cylinders at subcritical Reynolds numbers, and for specific cases, like a group of mixed large and smaller structures [6]. The latter work [6] numerically investigates fluid force coefficients and observes the vortex formation pattern on three identical rigid circular cylinders in proximity to a square cylinder. A parametric study is conducted in [7] for three identical stationary circular and D-shaped cylinders placed close to a square cylinder at Reynolds number 3900 in both linearly and parabolic sheared flows.

Considering the impact of cross-sectional shapes further, a numerical study is conducted by [8] for a flow over six identical stationary cylinders having different cross-sectional shapes at Reynolds number of 2.5×10^5 in the uniform and linearly sheared flow. Rectangular cylinders are investigated in details in [9, 10, 11], where one of the most impactful factors for hydrodynamic loads is the aspect ratio of rectangle sides. The works [9, 10] provide new experimental data and attempt to develop semi-empirical methods of predicting the response of structures. Further steps in improving the modelling approaches for the structural vibration of rectangle-shaped objects under the hydrodynamic excitation are performed in [11]. Another branch of studies considers a flow over a sphere [12, 13, 14], while still leaving issues of the impact of the cross-sectional shape of subsea structures open.

Further research on diverse cross-sectional shapes is performed in [15, 16, 17], where triangular and diamond cross-sections are studied in comparison. Research [15] is focused on the sensitivity to the corner sharpness for the diamond (rhomb) cross-section. Work [16] investigates effects from diverse cross-sections for the system with a rotational degree of freedom, when subjected to flow-induced vibration, and study [17] uses cross-sectional shapes for the energy harvesting with fluid-structure interaction.

Following published results, the current work aims to investigate the drag reduction when three structures of different cross-sectional shapes are located around a circular cylinder to observe the wake interference and the vortex formation pattern between these structures for the spacing ratio L/D varying from 1.67 to 2.83 in the uniform flow at the Reynolds number of 2.5×10^5 with the computational fluid dynamics approach. Specifically, the drag reducing ability of the upstream structure is of the research interest. The considered layout is a combination of cylinders placed in tandem, side-by-side and staggered position, with a mixture of cross-sectional shapes.

Materials and Methods. A system of four cylinders with a diameter (characteristic size) of 0.3 m with different cross-sectional types is considered in this study. The selected cross-sectional shapes and positions of structures are shown in Figure 1. Fluid forces and the flow interference are studied for the spacing ratio of L/D varying from 1.67 to 2.83 in the uniform current at the Reynolds number of 2.5×10^5 and the corresponding velocity of 0.837 m/s. The study focuses on the specific layout, where structures are positioned relative to each other in a mixed tandem (cylinders 1 and 3), side-by-side (cylinders 2 and 3, and cylinders 3 and 4) and staggered (cylinders 1 and 2, and cylinders 1 and 4) configuration. Cross-sectional shapes considered include half-circle, square, circle, and diamond.

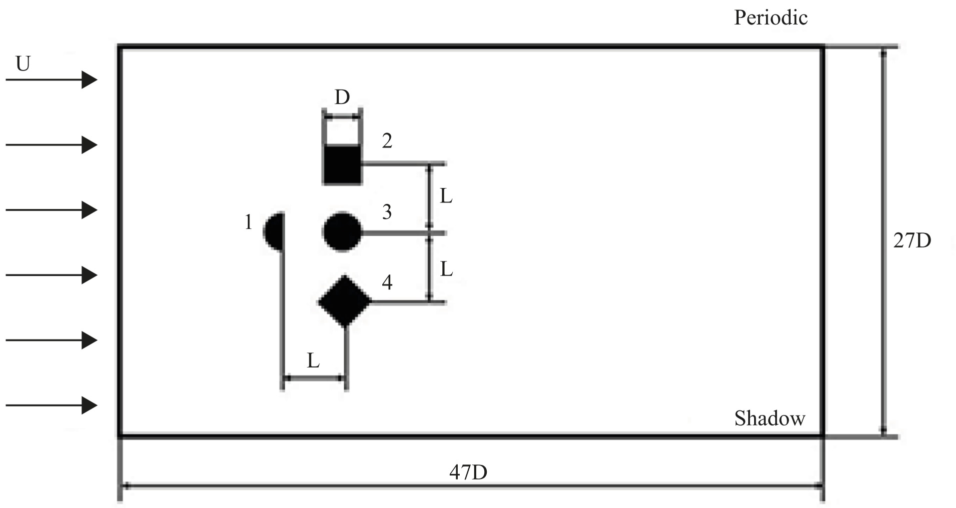


Fig. 1. Considered structures in the computational fluid domain

Computational fluid dynamic simulations are performed in the domain with a size of 47D x 27D. The top and bottom boundaries are located at a distance of 13.5D away from the center of the circular cylinder, periodic and shadow properties are assigned to these boundaries. The left boundary serves as a velocity-inlet, which is located at the distance of 20D from the centre of the circular structure 3 in the domain. The value of gauge pressure is set to zero at the pressure-outlet set at the right boundary. No-slip conditions are applied to the cylinders.

The flow around cylinders is simulated using the computational fluid dynamics software ANSYS Fluent, where the finite volume method is implemented to solve the Navier-Stokes system. The incompressible flow is considered, and the 2D DES transient simulations are conducted with the *k*–ω SST turbulence model. Time integration is performed using the second-order implicit transient formulation with a time step of 0.01 s, and the PISO algorithm is used as the solver.

The DES approach connects capabilities of the Reynolds-Averaged Navier-Stokes (RANS) and Large Eddy Simulation (LES) methods [8]. The RANS governing equations for the incompressible flow are as follows:

$$\frac{\partial\left(\rho\overline{u_i}\right)}{\partial x_i}=0, \tag{1}$$

$$\frac{\partial\left(\rho\overline{u_i}\right)}{\partial t}+\frac{\partial}{\partial x_i}\left(\rho\overline{u_i\,u_j}+\rho\overline{u_i^{'}u_j^{'}}\right)=\frac{\partial\overline{\rho}}{\partial x_i}+\frac{\partial\overline{\tau_{ij}}}{\partial x_j}, \tag{2}$$

where p is mean pressure, $\overline{u_i}$ is average Cartesian components of the velocity vector, $\rho\overline{u_i^{'}u_j^{'}}$ are Reynolds stresses, ρ is density of the fluid and $\overline{\tau_{ij}}$ is mean viscous stress vector components, which could be expressed as:

$$\partial\overline{\tau_{ij}}=\mu\left(\frac{\partial\overline{u_i}}{\partial x_j}+\frac{\partial\overline{u_j}}{\partial x_i}\right), \tag{3}$$

where μ is dynamic viscosity.

The Large Eddy Simulation (LES) system of equations for the incompressible flow can be written in the following way:

$$\frac{\partial\overline{u_i}}{\partial x_i}=0, \tag{4}$$

$$\frac{\partial\overline{u_i}}{\partial t}+\frac{\partial}{\partial x_j}\left(u_i\,u_j\right)=-\frac{1}{\rho}\frac{\partial\overline{\rho}}{\partial x_i}+v\frac{\partial^2\overline{u_i}}{\partial x_j\partial x_j}-\frac{\partial\overline{\tau_{ij}}}{\partial x_j}, \tag{5}$$

where $\overline{u_i}$ and $\overline{\rho}$ represent the resolved filtered velocity and pressure, respectively.

The diffusion term of the DES model is given by

$$Y_k=\rho\beta^{*}k\omega F_{DES}, \tag{6}$$

where β^{*} is a constant, *k* stands for fluctuation of the turbulent kinetic energy, ω is specific energy dissipation rate, and F_{DES} is as follows:

$$F_{DES}=max\left(\frac{L_t}{C_{des}\Delta_{max}},1\right), \tag{7}$$

where C_{des} is a constant, Δ_{max} is local maximum grid map $\Delta = (\Delta_1, \Delta_2, \Delta_3)^{1/3}$. Further, L_t is turbulent length scale:

$$L_t = \frac{\sqrt{k}}{\beta^* \omega}. \quad (8)$$

The DES-SST model uses the following zonal formulation:

$$F_{DES} = max\left(\frac{L_t}{C_{des}\Delta_{max}}\left(1 - F_{SST}\right), 1\right), \quad (9)$$

where $F_{SST} = 0$, F_1, F_2, and F_1, F_2 are mixed functions of the SST model.

Table 1 below provides results of the mesh independence test for the uniform flow of $\mathrm{Re} = 2.5\times10^5$. The mesh settings are adopted from [7], and the accuracy of the grid is demonstrated by comparisons in Table 1. All subsequent analysis in this paper is performed with Mesh 2, and the results include signals and frequencies of the fluid force coefficients and an indication of the vortex shedding pattern. The drag force fluctuations are presented in this work in terms of the drag force coefficient C_D which comprises the mean drag coefficient C_{D0} and the fluctuating drag coefficient C_D^{fl}, as follows:

$$C_D = C_{D0} + C_D^{fl}. \quad (10)$$

The lift force fluctuations are presented using the lift coefficient C_L.

Table 1

Mesh independence test results

Cases	C_{D0}	Number of cells	Strouhal number
$\mathrm{Re} = 2.5\times10^5$			
Current study			
Mesh 1	0.98	63,345	0.24
Mesh 2	1.08	86,478	0.24
Mesh 3	1.08	131,041	0.24
Published data			
Lehmkuhl, et al. (2014) (LES) [18]	0.833	–	0.238
Achenbach&Heinecke (1981) (Experiment) [19]	1.135	–	0.230
Re = 3,900			
Current study, Mesh 2	0.93	86,478	0.18
Wornom, et al. (2011) (VMS-LES) [20]	0.99	–	–
$\mathrm{Re} = 3.6\times10^6$			
Current study, Mesh 2	0.4100	86,478	–
Porteous, et al. (2015) (URANS) [21]	0.4206	–	–
Nazvanova, et al. (2022) (URANS) [22]	0.4657	74,496	–

Results. In this study, simulations are performed in two series. The first series is focused on recognising the overall effect of various cross-sectional shapes, placed at $L/D = 2.00$ from each other. Cylinder numbers here correspond to the ones used in Figure 1, according to the cylinders position. The calculation results for this set are reported in Table 2, in comparison to the case of structures with mixed cross-sections. The second series provides an insight into the impact of L/D ratio on hydrodynamic loads observed for the mixed cross-section case only, as in Figure 1. These results are summarised in Table 3 and allow defining the drag reducing effect of the D-shape upstream structure on loads when cross-sections are different.

Table 2

Simulation results for the same arrangement with different cross-sectional shapes for L/D = 2.00

L/D = 2.0	Basic case of structures with alternate cross-sections in Fig. 1	All circular structures	All square structures	All D-shaped structures	All diamond-shaped structures
Cylinder 1					
C_{D0}	0.45	0.28	0.49	0.48	0.46
C_D^{fl}	0.19	0.14	0.43	0.28	0.17
C_L	0.18	0.04	0.07	0.13	0.28
Cylinder 2					
C_{D0}	0.87	0.39	0.89	0.64	0.70
C_D^{fl}	1.03	0.38	1.38	0.49	0.60
C_L	1.38	0.53	0.07	0.11	0.07
Cylinder 3					
C_{D0}	0.3	0.24	0.26	0.35	0.70
C_D^{fl}	0.45	0.37	0.91	0.68	0.63
C_L	1.03	0.73	1.26	0.30	0.73
Cylinder 4					
C_{D0}	0.98	0.39	0.83	0.61	0.99
C_D^{fl}	0.90	0.27	0.96	0.44	1.05
C_L	1.22	0.81	1.63	0.37	1.11

Table 3

Simulation results for the mixed cross-sections at various L/D ratio

L/D	Cylinder 1			Cylinder 2			Cylinder 3			Cylinder 4		
	C_{D0}	C_D^{fl}	C_L	C_{D0}	C_D^{fl}	C_L	C_{D0}	C_D^{fl}	C_L	C_{D0}	C_D^{fl}	C_L
1.67	0.14	0.18	0.15	0.98	1.17	1.44	0.48	0.57	0.66	0.93	0.75	1.13
1.83	0.33	0.21	0.18	0.93	1.54	1.40	0.33	0.50	0.86	1.01	1.36	1.15
2.00	0.45	0.19	0.18	0.87	1.03	1.38	0.30	0.45	1.03	0.98	0.90	1.22
2.17	0.49	0.05	0.19	0.81	0.14	1.11	0.25	0.06	0.83	0.96	0.38	1.10
2.33	0.37	0.12	0.00	0.78	0.34	1.03	0.25	0.06	0.28	1.00	0.07	0.79
2.50	0.57	0.16	0.20	0.76	0.89	1.18	0.26	0.47	0.77	1.01	0.64	1.06
2.67	0.57	0.02	0.27	0.78	0.16	1.37	0.28	0.08	0.82	1.02	0.03	0.96
2.83	0.58	0.21	0.21	0.84	0.91	1.70	0.20	0.52	1.16	0.93	0.68	1.03

Comparison of all circular, all square, mixed (as in Fig. 1), all diamond and all D-shapes with each other in Table 2 reveals relatively lower hydrodynamic loads for all four structures observed for the circular shapes at the L/D = 2.00. The largest mean drag coefficient here is experienced by the fourth structure in both mixed-shaped and all diamond-shaped arrangement. The highest maximum fluctuating drag coefficient of 1.38 is observed for cylinder 2 in the all square-shaped arrangement. The largest maximum amplitude of the lift coefficient of 1.63 also belongs to the all square-shaped arrangement, but corresponds to cylinder 4. Mixed-shaped arrangement (or basic case of structures with alternate cross-sections, as in Fig. 1) at L/D = 2.00 demonstrates a relative consistency in large amplitudes of the lift coefficient for cylinders 2, 3, 4, which makes estimations of hydrodynamic loads for this arrangement more important, due to higher expected loads.

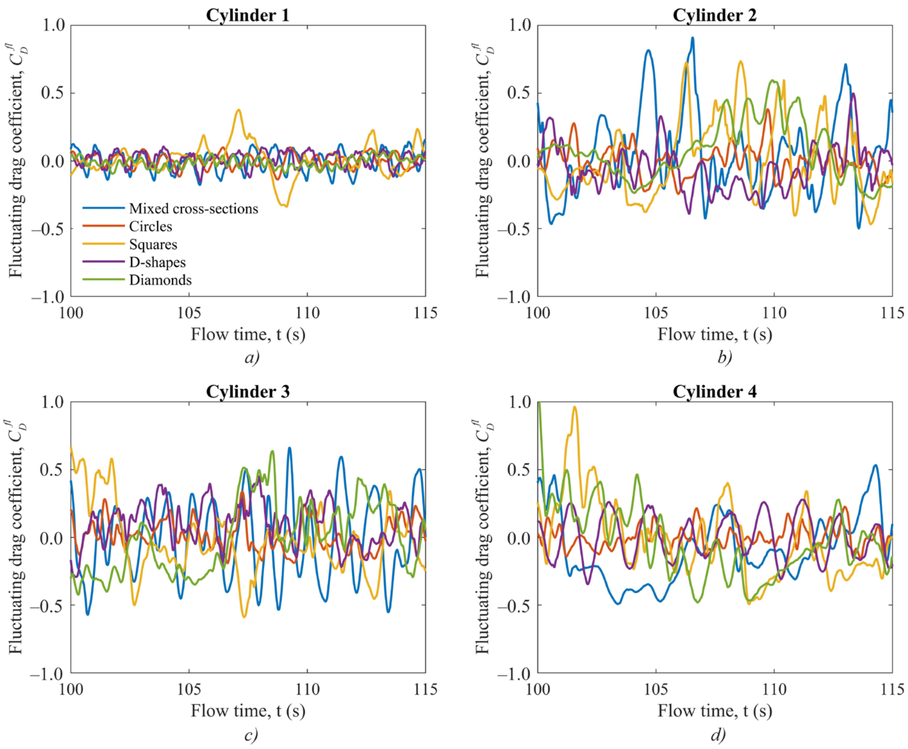


Fig. 2. Time histories of fluctuating drag coefficients for four cylinders of a different cross-sectional shape with L/D = 2.0:
a — cylinder 1; *b* — cylinder 2; *c* — cylinder 3; *d* — cylinder 4

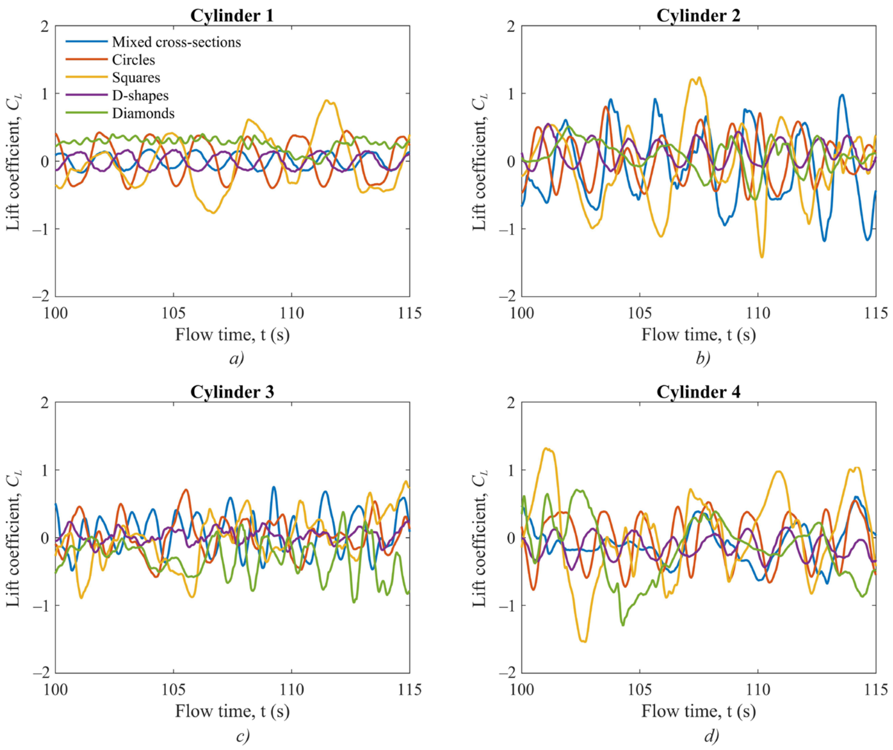


Fig. 3. Time histories of lift coefficients for four cylinders of a different cross-sectional shape with L/D = 2.0:
a — cylinder 1; *b* — cylinder 2; *c* — cylinder 3; *d* — cylinder 4

Further observation of signals of the fluctuating drag and lift coefficient in Figures 2 and 3 reveals meaningful instabilities in forces experienced by all structures with square shapes, and for structures 2, 3, 4 with diamond and mixed shapes. The comparison shows that circular and D-shaped structures would experience lower and more stable fluid loads in this arrangement. Table 2 and Figures 2 and 3 confirm that cylinder 1 in the shape of a circle or D-shape provides reducing fluid loads for the three downstream cylinders. This substantiates the common interest in further exploration of the effect of the D-shaped structure on reducing the drag force in the arrangement with all alternative cross-sectional shapes.

This effect is studied in details in the next (second) simulation series, presented for each cylinder in Figures 4–7 in terms of the fluid forces and in Figures 8, 9 — in terms of the fluid flow characteristics for the considered computational domain. Figure 4 illustrates fluid loads on the upstream structure, where the most unstable signal (at *L*/*D* = 2.17) belongs to fluctuations of the drag force. Figure 4 *c* also indicates presence of multiple frequencies in signals of the fluctuating drag coefficient, while a single dominating frequency can be identified for the lift force coefficient in Figure 4 *d*. Figures 4 *c* and 4 *d* demonstrate that the frequency of both lift and drag forces generally increases with the growing *L*/*D* ratio, and the maximum frequency is indicated by signals at *L*/*D* = 2.67 and 2.83.

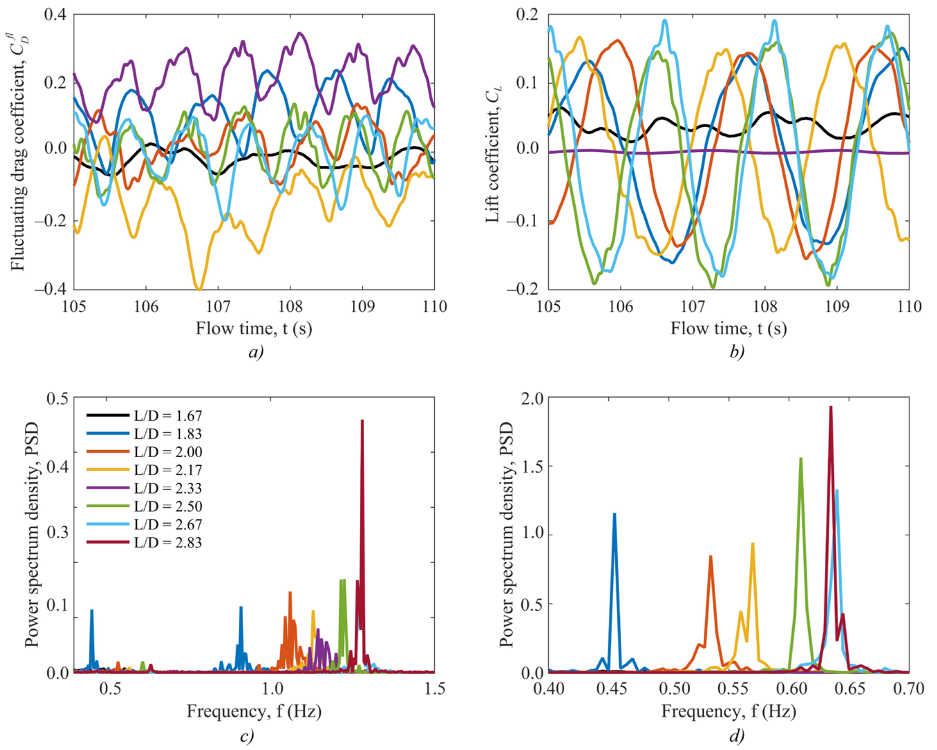


Fig. 4. Time histories of fluid force coefficients for cylinder 1 in the uniform flow:
a — fluctuating drag coefficient; *b* — lift coefficient; *c* — fluctuating drag coefficient FFT; *d* — lift coefficient FFT

Relatively similar complexity of frequencies of the lift force is observed in Figure 6 *d* for cylinder 3, where one to two dominant frequencies could be clearly identified. At the same time, more than two frequencies are observed in Figure 6 *c* for each signal of the fluctuating drag force. The pattern of growth in the overall dominant frequency with the increasing *L*/*D* is still recognisable for cylinder 3, similar to cylinder 1. Combination of frequencies is even more complex for cylinders 2 and 4, as comes from Figures 5 *c*–*d* and 7 *c*–*d*, this is not possible to indicate clear dependences in the frequencies of the fluctuating drag force. Some resemblance of the found growth trend could be still observed in Figure 5 *d* for the lift force coefficient for cylinder 2. This provides evidence for the generally unstable nature of hydrodynamic loads acting on the square cross-section shown in Figure 5.

Impact of the *L*/*D* ratio on the mean drag coefficient for cylinder 1, based on Table 3, is partially confirmed: apart from a couple of deviations, the mean drag force increases with the growth of *L*/*D*. Data for cylinders 2 and 4 do not indicate a specific pattern, as the values fluctuate back and forth within 10% from the initial mean drag coefficient at the smallest *L*/*D*. Cylinder 3, on the contrary, indicates a stable pattern of the reduced mean drag coefficient with the increased *L*/*D*, so that the reducing ability of the upstream D-shaped structure is evident, but for the central cylinder only. The largest mean drag coefficient of 1.02 is linked to cylinder 4 at *L*/*D* = 2.67. The considered range of *L*/*D* allows observing an important transition from the strong to minor interference in the wake of the three paired structures.

The highest fluctuating drag coefficients of 1.54 and 1.36 are linked to cylinders 2 and 4, respectively, both observed at *L*/*D* = 1.83. The feature of the maximum amplitude of the fluctuating drag coefficient, indicated in Table 2, is in absence of a specific dependence from the *L*/*D*, the values rapidly change from near zero to relatively high with a small increment of change in the ratio. The fluctuating drag coefficient has generally the lowest amplitudes for cylinder 1, average amplitudes — for cylinder 3, and the largest amplitudes — for cylinders 2 and 4.

The largest maximum amplitude of the lift coefficient occurs at *L*/*D* = 2.83 for cylinder 2. The lift coefficient generally resembles the distribution, similar to the maximum amplitude found for the fluctuating drag coefficient: the lift force appears to be the smallest for cylinder 1, relatively intermediate — for cylinder 3, and the highest — for cylinders 2 and 4, with no specific pattern linked to the *L*/*D* increase and reduction. This allows us to conclude that the ability to

reduce hydrodynamic forces by placing the upstream D-shaped structure in front of the array is limited. The force reduction is observed mainly for the structure placed in tandem downstream, and the effect is most pronounced for the mean drag coefficient, with some reduced effects also seen for the fluctuating drag and lift coefficients.

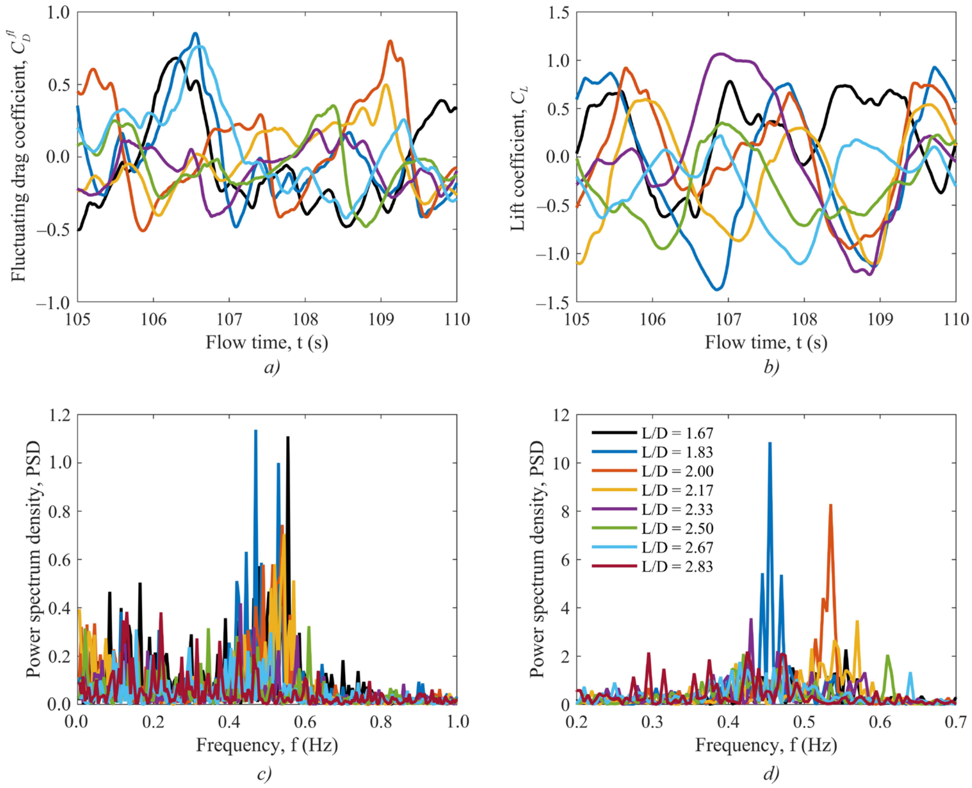


Fig. 5. Time histories of fluid force coefficients for cylinder 2 in the uniform flow:
a — fluctuating drag coefficient; *b* — lift coefficient; *c* — fluctuating drag coefficient FFT; *d* — lift coefficient FFT

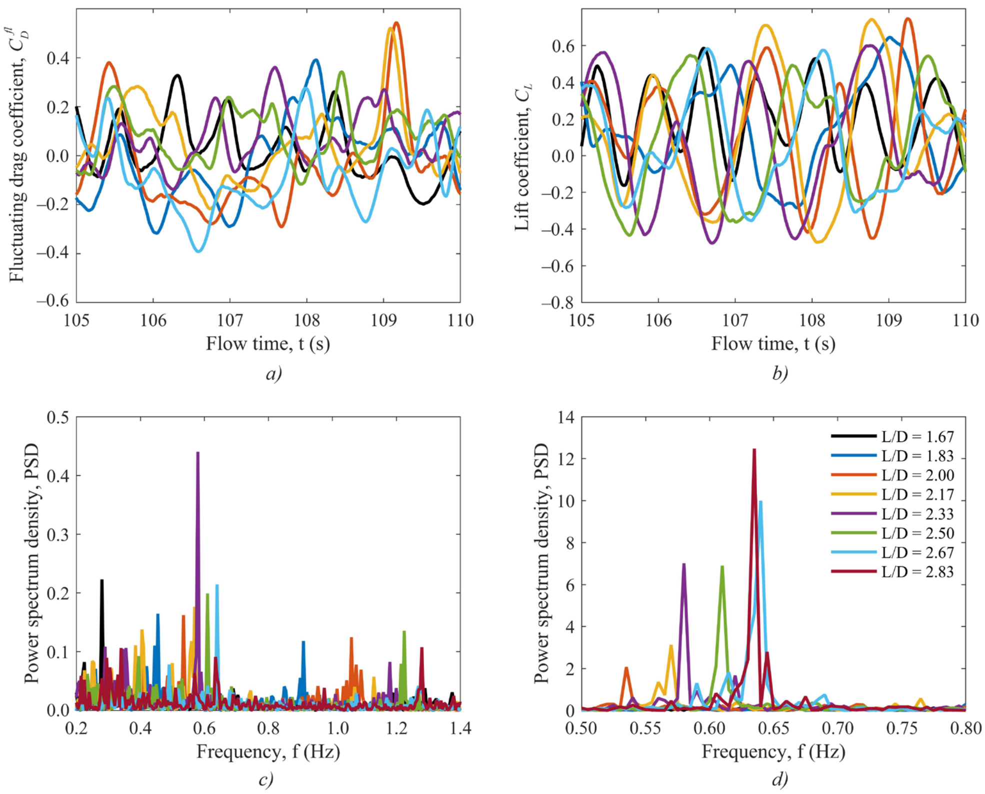


Fig. 6. Time histories of fluid force coefficients for cylinder 3 in the uniform flow:
a — fluctuating drag coefficient; *b* — lift coefficient; *c* — fluctuating drag coefficient FFT; *d* — lift coefficient FF

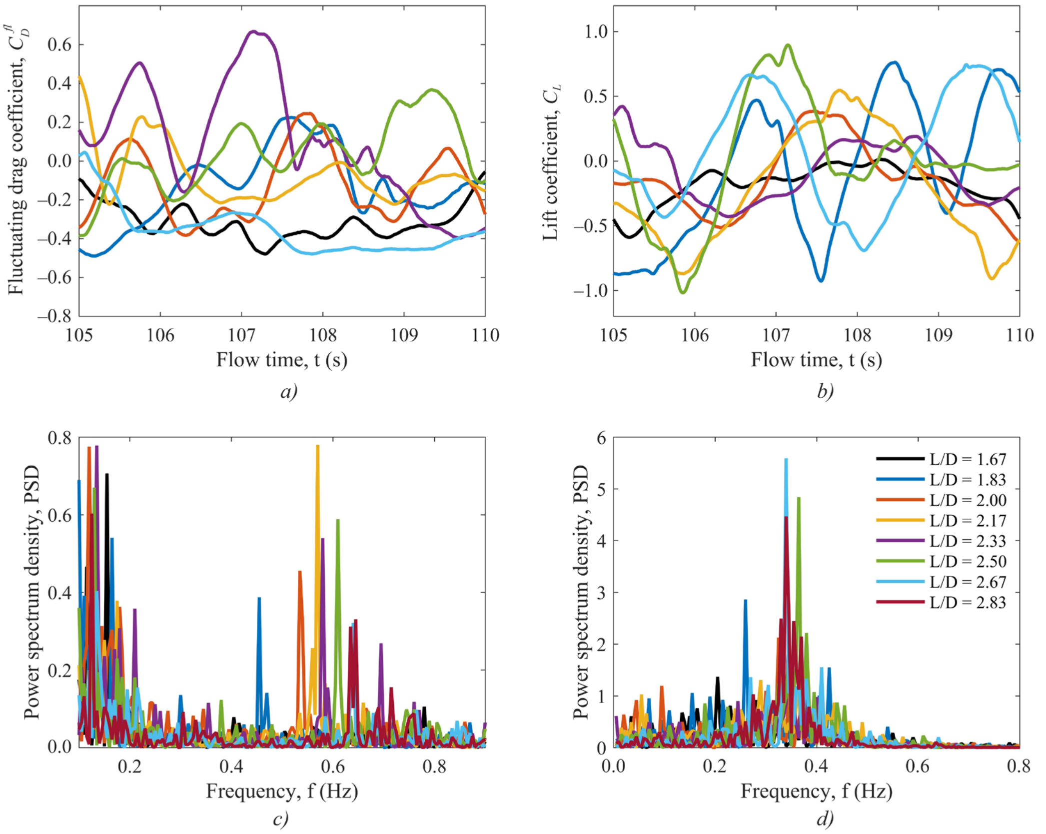


Fig. 7. Time histories of fluid force coefficients for cylinder 4 in the uniform flow:
a — fluctuating drag coefficient; *b* — lift coefficient; *c* — fluctuating drag coefficient FFT; *d* — lift coefficient FFT

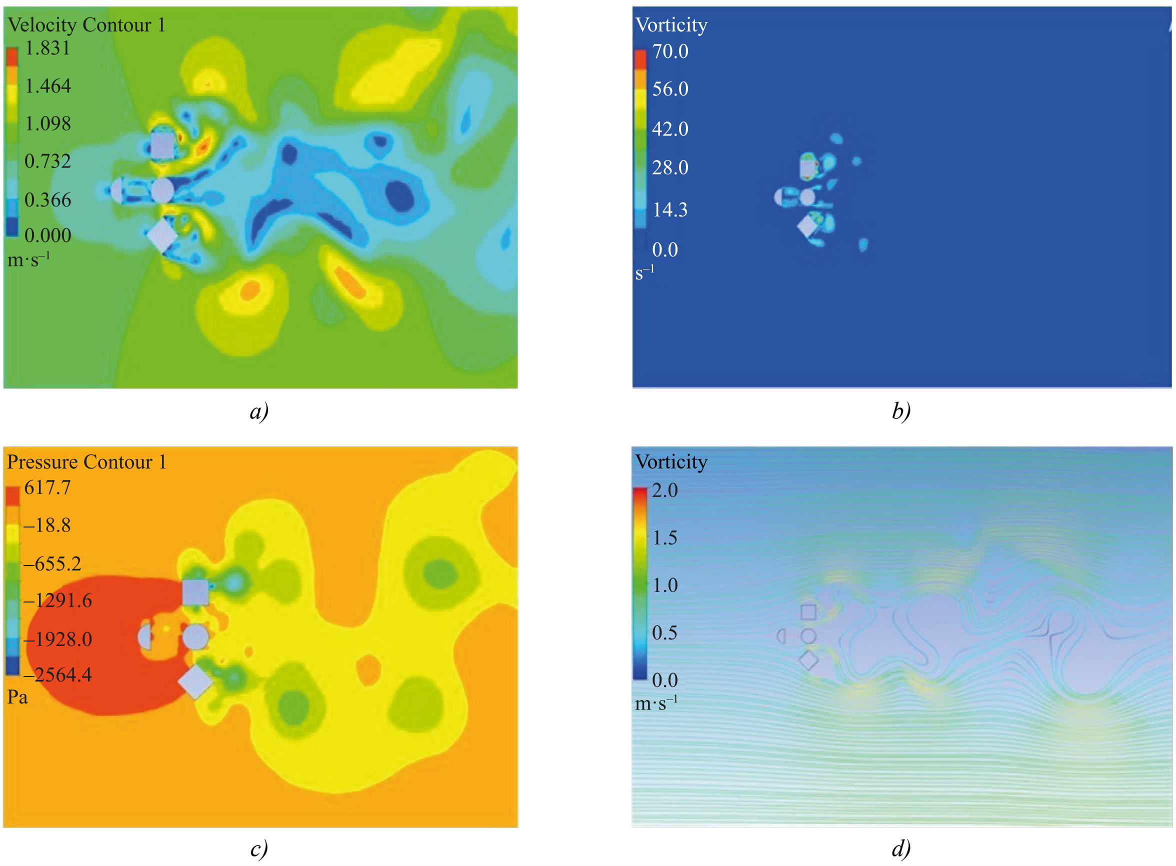


Fig. 8. Contours of the flow characteristics for L/D = 1.67 at 200 seconds:
a — velocity contour; *b* — vorticity contour; *c* — pressure contour; *d* — streamline

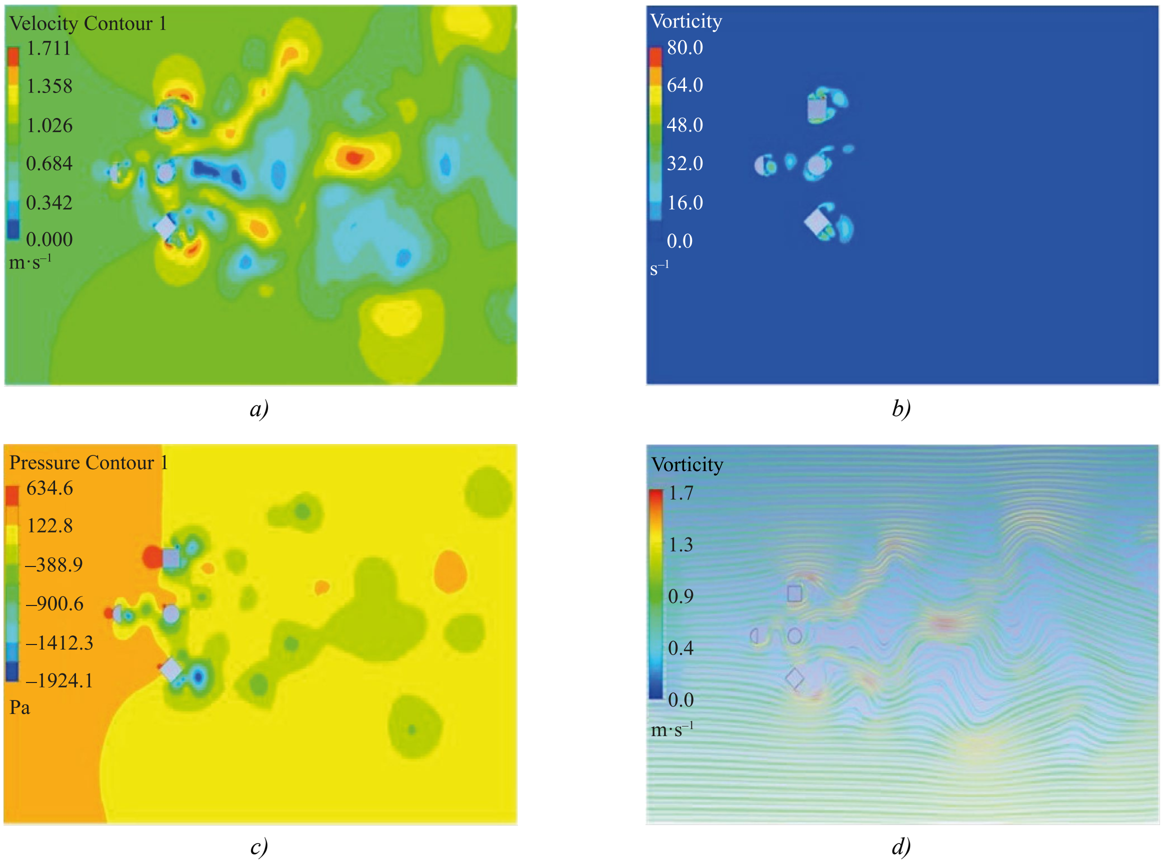


Fig. 9. Contours of the flow characteristics for *L*/*D* = 2.83 at 200 seconds:
a — velocity contour; *b* — vorticity contour; *c* — pressure contour; *d* — streamline

Figures 8–9 show the velocity, vorticity, pressure and streamlines of the flow around cylinders for some selected *L*/*D*, where both proximity and wake interference among the cylinders are presented for the time step of 200 s. The flow around cylinders is complex, and vortex formation patterns are highly affected, as the distance between the cylinders increases. The proximity interference is observed for cylinders 2, 3, and 4, alternate single vortices are shed on the downstream side of these structures. For the wake interference at *L*/*D* = 1.67, free shear layers separate from the upstream cylinder 1 and reattach themselves to the upstream side of cylinder 3, and a vortex street is only formed at the downstream side of cylinder 3. At this distance, a broad region of wake is created at the downstream side of cylinders 2, 3, and 4. As the *L*/*D* increases above 2.00, there are vortices formed at the upstream side of cylinder 3, in the wake of cylinder 1. A vortex street is also formed at the downstream side of cylinder 3, with formation of 2S vortices. Figures 8 *a*, 9 *c* demonstrate a group of minor vortices formed following the diamond-shaped cylinder 4 and a vortex pair formed in a similar to S+P vortex cycle past cylinder 2.

Discussion and Conclusion. The 2D numerical simulations are performed in this work for cylinders with different cross-sectional shapes at the Reynolds number of 2.5×10^5 using the DES approach. The considered cylinders are studied in a complex position of an upstream D-shaped structure in front of three paired structures, with the aim to investigate the drag-reducing ability of this specific layout, observe the flow complexity, the wake interference from each structure, and vortex formation patterns.

The following conclusions could be made from this study:

1. The ability to reduce hydrodynamic forces by placing the upstream D-shaped structure is mainly limited to the structure placed in tandem downstream, and the effect is most pronounced for the mean drag coefficient.

2. Overall, the mean drag coefficient of cylinders is observed to be affected by varying *L*/*D*, with the main effect on the mean drag coefficient of cylinder 1, which grows with increasing *L*/*D*, and of cylinder 3, which reduces with increasing *L*/*D*.

3. Competition of frequencies is observed for the fluctuating drag coefficient for all structures and lift coefficient signal of cylinders 2 and 4. This competition is due to the joint effects of both the uniform current and wake interference, which intensifies at a lower *L*/*D* in terms of changes to the resulting vortex street.

4. Both proximity and wake interference among the cylinders are observed. The flow around cylinders is complex, and vortex formation patterns are highly affected as the distance between the cylinders increased with 2S being the major vortex type formed and shedding the additional vortices from the square and diamond structures.

The study generally contributes to the field of knowledge by advancing our understanding of fluid-structure interactions, drag reduction strategies, and vortex dynamics, with potential applications in offshore energy systems. The current work contributes to the development of the drag reduction strategies through analyzing the impact of the upstream D-shaped structure on downstream cylinders. Understanding how different structural configurations affect drag can inform the design of more efficient systems in various engineering applications, such as subsea transportation of fluids. By observing flow complexity, wake interference, and vortex formation patterns, this study contributes to the understanding of fluid dynamics around complex geometries. This knowledge is crucial for optimizing the performance of structures in environments where fluid flow plays a significant role, such as subsea engineering. The results of the present research highlight the effect of varying the aspect ratio L/D on drag coefficients to inform engineering designs of similar arrangements. This study reveals the intricate vortex dynamics and shedding patterns, particularly concerning the proximity and wake interference among cylinders. Understanding these phenomena can aid in predicting and controlling flow behavior around complex configurations, leading to more efficient designs and better performance in practical applications in offshore systems.

References

1. Zdravkovich MM. Review of Flow Interference between Two Circular Cylinders in Various Arrangements. *Journal of Fluids Engineering.* 1977;99(4):618–633. https://doi.org/10.1115/1.3448871

2. Williamson CHK. Vortex Dynamics in the Cylinder Wake. *Annual Review of Fluid Mechanics.* 1996;28(1):477–539. https://doi.org/10.1146/annurev.fl.28.010196.002401

3. Wanhai Xu, Haokai Wu, Kun Jia, Enhao Wang. Numerical Investigation into the Effect of Spacing on the Flow-Induced Vibrations of Two Tandem Circular Cylinders at Subcritical Reynolds Numbers. *Ocean Engineering*. 2021;236:109521. https://doi.org/10.1016/j.oceaneng.2021.109521

4. Sumner D, Richards MD, Akosile OO. Two Staggered Circular Cylinders of Equal Diameter in Cross-Flow. *Journal of Fluids and Structures*. 2005;20(2):255–276. https://doi.org/10.1016/j.jfluidstructs.2004.10.006

5. Bearman PW, Wadcock AJ. The Interaction between a Pair of Circular Cylinders Normal to a Stream. *Journal of Fluid Mechanics*. 1973;61(3):499–511. https://doi.org/10.1017/S0022112073000832

6. Annapeh HF, Kurushina V. Numerical Simulation of Flow-Induced Forces on Subsea Structures in a Group Under Uniform and Sheared Flow. In book: Dimitrovová Z, Biswas P, Gonçalves R, Silva T. (eds). *Recent Trends in Wave Mechanics and Vibrations*. Cham: Springer; 2022. P. 512–522. https://doi.org/10.1007/978-3-031-15758-5_52

7. Annapeh HF, Kurushina V. Flow-Induced Forces for a Group of One Large and Several Small Structures in the Sheared Turbulent Flow. *Fluids*. 2023;8(5):158. https://doi.org/10.3390/fluids8050158

8. Annapeh HF, Kurushina V. Hydrodynamic Loads on a Group of Six Structures of Different Cross-Sections in Uniform and Sheared Flow. *Journal of Marine Science and Engineering*. 2023;11(2):383. https://doi.org/10.3390/jmse11020383

9. Mannini C, Marra AM, Massai T, Bartoli G. Interference of Vortex-Induced Vibration and Transverse Galloping for a Rectangular Cylinder. *Journal of Fluids and Structures*. 2016;66:403–423. https://doi.org/10.1016/j.jfluidstructs.2016.08.002

10. Marra AM, Mannini C, Bartoli G. Measurements and Improved Model of Vortex-Induced Vibration for an Elongated Rectangular Cylinder. *Journal of Wind Engineering and Industrial Aerodynamics*. 2015;147:358–367. https://doi.org/10.1016/j.jweia.2015.08.007

11. Bin Liu, Renjie Jiang. Vortex-Induced Vibrations of a Rectangular Cylinder. *Ocean Engineering*. 2022;266:112883. https://doi.org/10.1016/j.oceaneng.2022.112883

12. Jauvtis N, Govardhan R, Williamson CHK. Multiple Modes of Vortex-Induced Vibration of a Sphere. *Journal of Fluids and Structures.*2001;15(3–4):555–563. https://doi.org/10.1006/jfls.2000.0348

13. Govardhan RN, Williamson CHK. Vortex-Induced Vibrations of a Sphere. *Journal of Fluid Mechanics*. 2005;531:11–47. https://doi.org/10.1017/S0022112005003757

14. Gabyshev DN, Szakáll M, Shcherbakov DV, Fedorets AA, Dyachkov SM. Oscillatory Signatures in the Raindrop Motion Relative to the Air Medium with Terminal Velocity. *Atmosphere.* 2022;13(7):1137. https://doi.org/10.3390/atmos13071137

15. Leontini JS, Thompson MC. Vortex-Induced Vibrations of a Diamond Cross-Section: Sensitivity to Corner Sharpness. *Journal of Fluids and Structures.* 2013;39:371–390. https://doi.org/10.1016/j.jfluidstructs.2013.01.002

16. Arionfard H, Mohammadi S. Numerical Investigation of the Geometrical Effect on Flow-Induced Vibration Performance of Pivoted Bodies. *Energies*. 2021;14(4):1128. https://doi.org/10.3390/en14041128

17. Mehdipour I, Madaro F, Rizzi F, De Vittorio M. Comprehensive Experimental Study on Bluff Body Shapes for Vortex-Induced Vibration Piezoelectric Energy Harvesting Mechanisms. *Energy Conversion and Management: X.* 2022;13:100174. https://doi.org/10.1016/j.ecmx.2021.100174

18. Lehmkuhl O, Rodríguez I, Borrell R, Chiva J, Oliva A. Unsteady Forces on a Circular Cylinder at Critical Reynolds Numbers. *Physics of Fluids.* 2014;26(12):125110. https://doi.org/10.1063/1.4904415

19. Achenbach E, Heinecke E. On Vortex Shedding from Smooth and Rough Cylinders in the Range of Reynolds Numbers 6×10^3 to 5×10^6. *Journal of Fluid Mechanics*. 2006;109:239–251. https://doi.org/10.1017/S002211208100102X

20. Wornom S, Ouvrard H, Salvetti MV, Koobus B, Dervieux A. Variational Multiscale Large-Eddy Simulations of the Flow past a Circular Cylinder: Reynolds Number Effects. *Computers & Fluids*. 2011;47(1):44–50. https://doi.org/10.1016/j.compfluid.2011.02.011

21. Porteous A, Habbit R, Colmenares J, Poroseva S, Murman SM. Simulations of Incompressible Separated Turbulent Flows around Two-Dimensional Bodies with URANS Models in OpenFOAM. In: *Proc. 22nd AIAA Computational Fluid Dynamics Conference.* Reston, VA: AIAA; 2015. P. 2609. https://doi.org/10.2514/6.2015-2609

22. Nazvanova A, Guang Yin, Muk Chen Ong. Numerical Investigation of Flow around Two Tandem Cylinders in the Upper Transition Reynolds Number Regime Using Modal Analysis. *Journal of Marine Science and Engineering*. 2022;10(10):1501. https://doi.org/10.3390/jmse10101501

About the Authors:

Henry Francis Annapeh, Research Assistant, Laboratory of Vibration and Hydrodynamics Modelling, Industrial University of Tyumen (38, Volodarskogo Str., Tyumen, 625000, Russian Federation), ORCID, ScopusID, kinghenry939@gmail.com

Victoria A. Kurushina, Head of the Laboratory of Vibration and Hydrodynamics Modelling, Industrial University of Tyumen (38, Volodarskogo Str., Tyumen, 625000, Russian Federation), SPIN-code: 7681–7930, ORCID, ScopusID, ResearcherID, v.kurushina@outlook.com

Об авторах:

Генри Франсис Аннапе, лаборант лаборатории вибрационного и гидродинамического моделирования Тюменского индустриального университета (625000, Российская Федерация, г. Тюмень, ул. Володарского, 38), ORCID, ScopusID, kinghenry939@gmail.com

Виктория Александровна Курушина, заведующий лаборатории вибрационного и гидродинамического моделирования Тюменского индустриального университета (625000, Российская Федерация, г. Тюмень, ул. Володарского, 38), SPIN-код: 7681–7930, ORCID, ScopusID, ResearcherID, v.kurushina@outlook.com

Claimed Contributorship:

HF Annapeh: conceptualization, literature review, methodology, investigation, computation, processing the results, original draft preparation, editing.

VA Kurushina: methodology, research management, investigation, computation, processing the results, financial backing, review and editing.

Заявленный вклад авторов:

Г.Ф. Аннапе: концептуализация, обзор литературы, методология, исследование, расчёты, обработка результатов, подготовка первого черновика статьи, редактирование.

В.А. Курушина: методология, руководство исследованием, расчёты, обработка результатов, финансирование, редактирование статьи.

Conflict of Interest Statement: **the authors declare no conflict of interest.**

Конфликт интересов: **авторы заявляют об отсутствии конфликта интересов.**

All authors have read and approved the final manuscript.

Все авторы прочитали и одобрили окончательный вариант рукописи.

Received / Поступила в редакцию 17.03.2024
Revised / Поступила после рецензирования 10.04.2024
Accepted / Принята к публикации 21.04.2024